

## Coronal Diagnostics from Narrowband Images around 30.4 nm

V. Andretta<sup>1</sup> · D. Telloni<sup>2</sup> · G. Del Zanna<sup>3</sup>

Received: 2 September 2011 / Accepted: 12 March 2012 / Published online: 5 April 2012

**Abstract** Images taken in the band centered at 30.4 nm are routinely used to map the radiance of the He II Ly  $\alpha$  line on the solar disk. That line is one of the strongest, if not the strongest, line in the EUV observed in the solar spectrum, and one of the few lines in that wavelength range providing information on the upper chromosphere or lower transition region. However, when observing the off-limb corona the contribution from the nearby Si XI 30.3 nm line can become significant. In this work we aim at estimating the relative contribution of those two lines in the solar corona around the minimum of solar activity. We combine measurements from CDS taken in August 2008 with temperature and density profiles from semiempirical models of the corona to compute the radiances of the two lines, and of other representative coronal lines (*e.g.*, Mg X 62.5 nm, Si XII 52.1 nm). Considering both diagnosed quantities from line ratios (temperatures and densities) and line radiances in absolute units, we obtain a good overall match between observations and models. We find that the Si XI line dominates the He II line from just above the limb up to  $\approx 2 R_{\odot}$  in streamers, while its contribution to narrowband imaging in the 30.4 nm band is expected to become smaller, even negligible in the corona beyond  $\approx 2 - 3 R_{\odot}$ , the precise value being strongly dependent on the coronal temperature profile.

**Keywords:** Corona – Spectrum, Ultraviolet – Spectral Line, Intensity and Diagnostics

### 1. Introduction

Narrowband imaging of the Sun in the EUV has become an almost indispensable tool for solar physicists. Instruments like the *Extreme UltraViolet Imaging Telescope* (EIT) onboard the *Solar and Heliospheric Observatory* (SOHO), and the

---

<sup>1</sup> INAF/Osservatorio Astronomico di Capodimonte, Salita Moiarriello 16, 80131 Napoli, Italy – email: andretta@oacn.inaf.it

<sup>2</sup> INAF/Osservatorio Astrofisico di Torino, Strada Osservatorio 20, 10025 Pino Torinese (TO), Italy – email: telloni@oato.inaf.it

<sup>3</sup> DAMTP, Centre for Mathematical Sciences, University of Cambridge, UK email: G.Del-Zanna@damtp.cam.ac.uk

*Atmospheric Imaging Assembly* (AIA) onboard the *Solar Dynamics Observatory* (SDO) routinely monitor the Sun at various wavelengths. Both instruments observe, among others, in bands centered around 30.4 nm, the wavelength of the Ly  $\alpha$  line of ionized helium.

Observations with the *Sounding CORona Experiment* (SCORE: Fineschi *et al.*, 2004; Fineschi, 2006), flown on HERSCHEL, a NASA sounding-rocket payload, also include such a band. Finally, the *Multi Element Telescope for Imaging and Spectroscopy* (METIS), one of the scientific payloads selected for *Solar Orbiter*, the M-class mission of the ESA Cosmic Vision program for the exploration of the Sun at a distance as close as 0.28 AU, will also have a spectro-imaging channel at that wavelength.

### 1.1. The Spectral Region around 30.4 nm

The most interesting line in the band around 30.4 nm is certainly the He II 30.4 nm, the Ly  $\alpha$  of ionized helium. Narrowband imaging of the solar disk around that line therefore allows probing relatively cool plasma ( $T < 10^5$  K) in the EUV, although the details of the formation of that line in the quiescent solar atmosphere are still somewhat controversial (*e.g.*, Andretta, Del Zanna, and Jordan, 2003; Pietarila and Judge, 2004).

However, for the extended corona, one of the most interesting diagnostics possible with the He II 30.4 nm line is related to a radiative “pumping” mechanism analogous to that exhibited by hydrogen Ly  $\alpha$ . Furthermore, the nearby strong Si XI resonance line at 30.3 nm adds the possibility of probing radial velocities in the range of  $\approx 400$  km s $^{-1}$  via a similar mechanism.

### 1.2. The Ratio Si XI 30.3 nm/He II 30.4 nm

The presence of the nearby Si XI line, while providing additional diagnostic opportunities, poses a problem for the interpretation of narrowband images. The ratio Si XI 30.3 nm/He II 30.4 nm is around 0.1 in the quiescent solar atmosphere seen on the solar disk (Del Zanna and Andretta, 2011), or even smaller in active regions (Thomas and Neupert, 1994), but dramatically changes in the corona above the limb.

To illustrate this, we show in Figure 1 the peak radiances of the two lines, measured from spectra taken with the *Normal Incidence Spectrograph* (NIS) of the SOHO/*Coronal Diagnostic Spectrometer* (CDS: Harrison *et al.*, 1995). The raster scans shown here were taken on 21 January 1998, and can be considered representative of relatively quiescent off-limb regions: only a small prominence is visible in the field of view (FOV). The ratio of the two lines is also shown.

The rapid increase of the ratio Si XI 30.3 nm/He II 30.4 nm above the limb is also apparent from the average profiles at various heights above the limb shown in Figure 1. However, data obtained from CDS/NIS are limited to the lower corona; it is entirely possible that further out in the corona the ratio Si XI 30.3 nm/He II 30.4 nm could decrease again. Whether and where that happens is of utmost relevance for the interpretation of narrowband imaging of the outer corona.

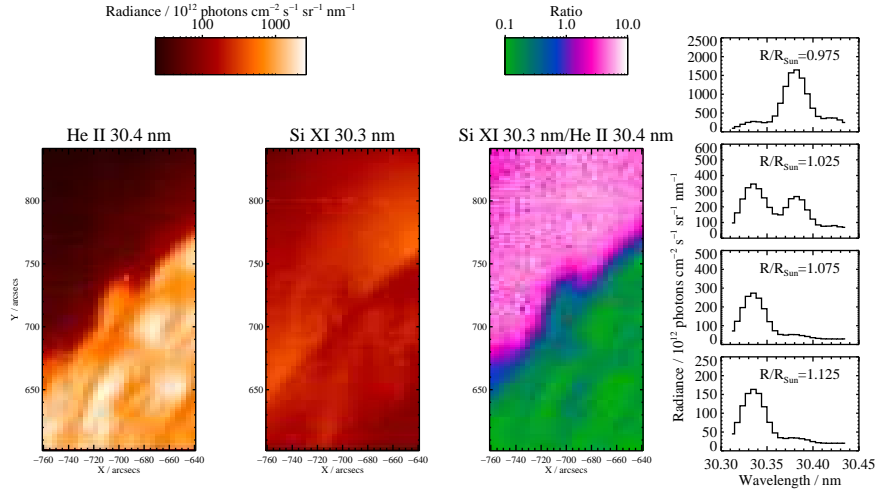


**Figure 1.** Images (leftmost two panels) of the He II 30.4 nm and Si XI 30.3 nm lines created from CDS spectral rasters, and their ratio. In the third panel, ratios coded with red/white indicate a high value of Si XI 30.3 nm/He II 30.4 nm, while green indicate a dominant He II 30.4 nm line. The average spectra around 30.4 nm at different heliocentric distances from the same data set are shown in the rightmost panels.

In this article we will make an estimate of the ratio of the two lines in typical conditions of the corona at solar minimum. Using observed EUV, spectrally resolved radiances from SOHO/CDS (Section 2), we will first estimate average on-disk and off-limb radiances in several coronal lines, including those for Si XI 30.3 nm and He II 30.4 nm; from the line ratios we will also derive average densities and temperatures in the corona. These measurements will then provide the input disk irradiance needed to calculate the radiative excitation of the coronal lines, as well as constraints to the calculations at the lower boundaries of the models, *i.e.* near the solar limb (Section 3).

## 2. SOHO/CDS Radiances

In order to derive both mean on-disk and off-limb radiances of lines in the spectral range observed by CDS/NIS, we used whole-Sun scans taken with the CDS/NIS study called USUN in the CDS database.

The CDS USUN study consists of 69 rasters, for a total of 700 to 1000 exposures with the 4'' slit, covering the whole Sun and part of the off-limb corona in about 13 hours. Further details on the CDS USUN study are given in Thompson and Brekke (2000) and Del Zanna and Andretta (2011). Here we use the data processed and analyzed as described in detail in the latter article, including the radiometric calibration of CDS/NIS of Del Zanna *et al.* (2001b, 2010). We note that the new calibration is significantly different from the previous ones. We also note that measurements of the He II 30.4 nm radiance/irradiance have been largely inconsistent throughout the literature, and that the Del Zanna and

Andretta (2011) calibration provides irradiances in agreement with the SDO *Extreme Ultraviolet Variability Experiment* (EVE) prototype measurements of 14 April 2008 as described in the same article. From comparisons between our measurements with those by various instruments, two errors in the analysis software of CDS and the *EUV Normal-Incidence Spectrometer* (EUNIS: Jordan and Brosius 2007) were uncovered (Wang *et al.*, 2011). Our CDS measurements are now also in agreement with the EUNIS ones, within a few percent.

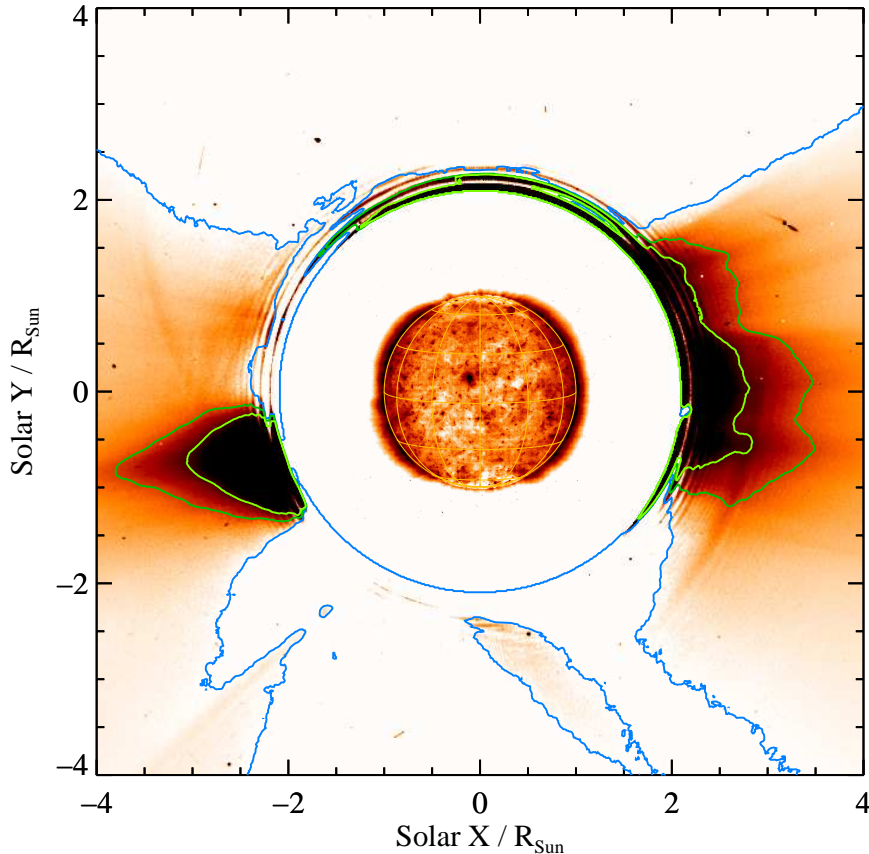


**Figure 2.** Image of the solar corona from SOHO/LASCO-C2, taken on 25 August 2008 07:29:36 UT, overlaid on a SOHO/EIT 195 image taken on the same day at 07:13:47 UT. A radial average of the corona has been subtracted from the LASCO image to enhance the contrast of coronal structures.

The CDS USUN scans have been taken approximately once a month starting in 1998. We chose to analyze a USUN scan taken on 25 August 2008, *i.e.* during the extended minimum between activity Cycles 23 and 24. The configuration of the corona from SOHO/EIT (Delaboudinière *et al.*, 1995) and from the C2 telescope of the *Large Angle and Spectrometric Coronagraph* (LASCO: Brueckner *et al.*, 1995) on that date is shown in Figure 2. For display clarity, an average radial profile has been subtracted from the LASCO-C2 image.

## 2.1. Selected Regions of the FOV

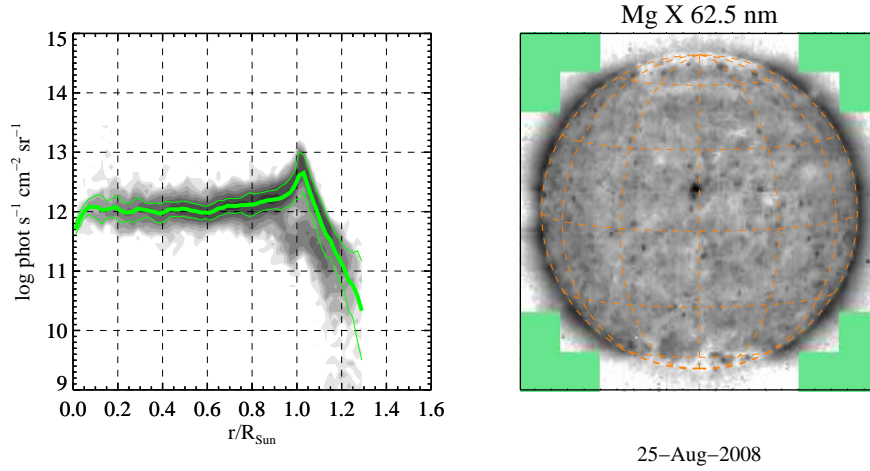


**Figure 3.** Right: Radiance of the Mg X 62.5 nm line from CDS/NIS observations; USUN study on 25 August 2008. Left: Histogram showing the distribution of radiances in the line as a function of heliocentric distance; green: median value (plus or minus one standard deviation).

For each line in the CDS spectral range, it is possible to build a monochromatic image of the Sun. An example is shown in the right-hand panel of Figure 3, for the Mg x 62.5 nm line. The solar disk on that date did not exhibit significant activity, while two symmetrical polar coronal holes are clearly visible.

For each monochromatic image, we then built a histogram of radiances as function of distance from the center of the Sun. An example of the two-dimensional histogram thus obtained is shown in the left-hand panel of Figure 3. We then obtained an average radiance radial profile from the median of the histograms at each heliocentric distance (thicker line in Figure 3). The standard deviation of the profile is also shown (thinner lines).

The same procedure can be applied to specific regions of the FOV. In particular, we selected the southeast quadrant of the disk, corresponding to the base of the streamer visible in Figure 2, and the two polar regions. The corresponding images and radiance histograms are shown in Figure 4. We have verified that the choice of a specific region of interest outside the polar coronal holes does not affect significantly the radiance radial profiles for most lines, a fact consistent with the very low activity state of the lower corona on that date.

## 2.2. Off-limb Radiances

There are at least two known sources of spurious radiation that can affect the measurement of off-limb line radiances in CDS.

First, radiation from the much brighter solar disk can be diffused into the tail of the instrument's point-spread function (PSF) to contribute to off-limb line radiation. Harrison *et al.* (1995) give values for the PSF (measured at 6.8 nm) of  $10^{-6.2}$  and  $10^{-6.6}$  for distances of  $100''$  and  $150''$ , respectively, from the core.

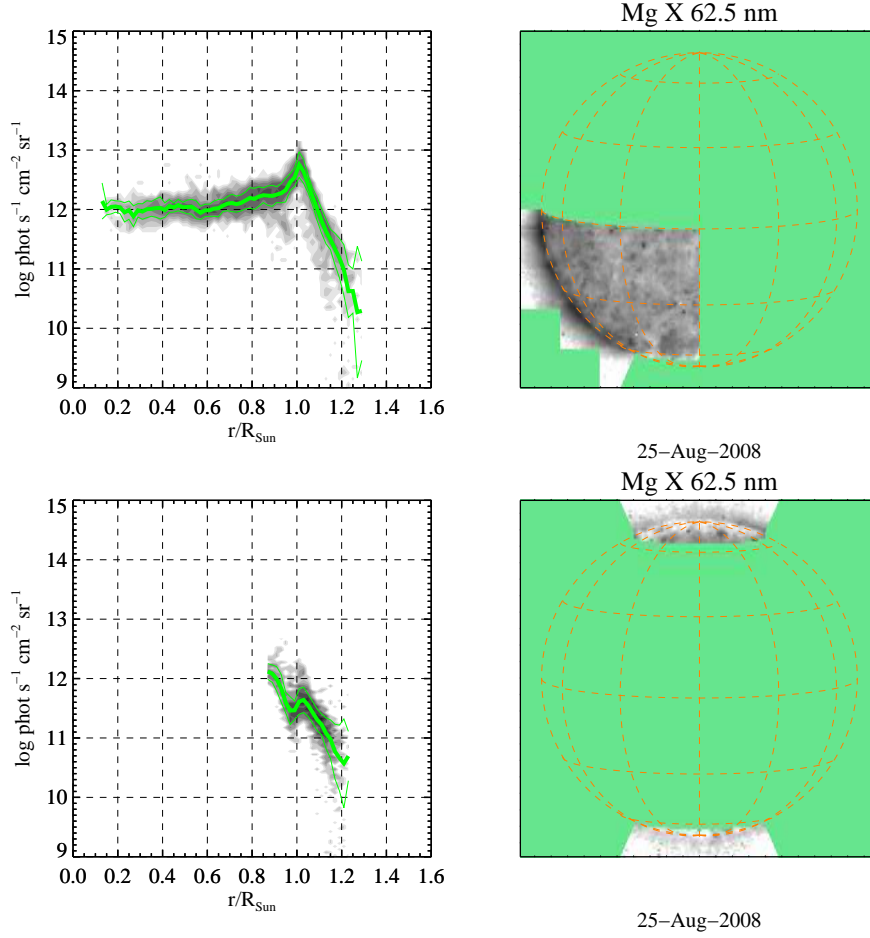


**Figure 4.** Right panels: Radiance of the Mg X 62.5 nm line from CDS/NIS observations, for selected regions of the FOV; USUN study on 25 August 2008. Left panels: Histograms showing the distribution of radiances in the line as a function of heliocentric distance; green: median value (plus or minus one standard deviation). Top panels: southeast quadrant, roughly corresponding to the base of the streamer shown in Figure 2; Bottom panels: polar regions (coronal holes).

Based on those figures, at distances of  $r \approx 1.2 R_{\odot}$  we would expect the fractional contribution of the disk to line radiances to be well below  $10^{-6}$ , compared to a decrease of the order of little more than a factor ten in typical coronal lines (Figures 3 and 4). However, the in-flight performance of the instrument is not necessarily as good as indicated by those laboratory measurements, especially after the loss of contact with the SOHO spacecraft in June 1998, which led to a significant alteration of the instrumental response.

To estimate the contribution of disk scattered radiation, we examined the off-limb behavior of the strongest cool lines (lines with formation temperature much less than  $10^6$  K) in the CDS range: He I 58.4 nm and O V 62.9 nm, assuming that the coronal contribution to their off-limb measured radiances is negligible (Figure

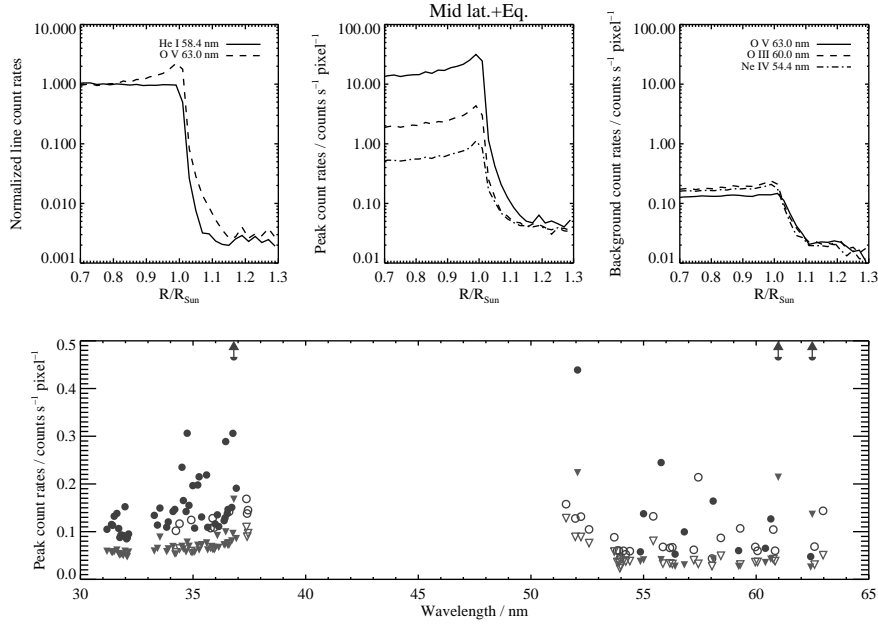


**Figure 5.** Radial profiles for the count rates of two of the strongest lines in the CDS range, averaged over equatorial and mid-latitude regions, and normalized to the mean line count rate over the solar disk (leftmost, upper panel). The other two plots in the upper row show, for three representative lines in the NIS 2 range with formation temperature below  $5 \times 10^5$  K, the average count rates in the line center pixel (center, upper panel), and in adjacent (background) pixels (rightmost, upper panel). The bottom panel shows the peak count rate per pixel for all of the lines detected in the CDS range *vs.* wavelength, averaged in the range  $1.05 < r/R_{\odot} < 1.15$  (circles) and  $r/R_{\odot} > 1.2$  (triangles). Open and filled symbols mark lines with formation temperature below and above  $5 \times 10^5$  K, respectively. The values for the strongest coronal lines (the Mg X doublet at 60.9 and 62.5 nm, Mg IX 36.8 nm) around  $r/R_{\odot} = 1.1$  are off the vertical scale, and thus are not shown here.

5, left panel in the upper row). From our data, it appears that the fractional contribution of disk scattered radiation is below  $3 \times 10^{-3}$  at  $r \approx 1.2 R_{\odot}$ .

A more precise determination of this contribution is impeded by the presence of a continuum background, only weakly dependent on wavelength (Thompson and Brekke, 2000). The source of this background is unclear; however, if of solar origin, its pattern of spatial variation on the disk would suggest a cool source (Figure 5, center and right panels in the upper row). According to Thompson and Brekke (2000), for instance, such a background is mainly due to Ly  $\alpha$  radiation scattered by the far wings of the grating profile, but with likely contributions from a variety of other lines. In any case, the presence of that background can hamper accurate measurement of off-limb lines, especially of the faintest ones.

The average line peak count rates at  $r \approx 1.25 R_{\odot}$  (average above  $1.2 R_{\odot}$ ), shown in the lower panel of Figure 5 (triangles), clearly outline the background continuum; only a few strong lines are still measurably above that level. In contrast, at  $r \approx 1.1 R_{\odot}$  (average between  $1.05$  and  $1.15 R_{\odot}$ ), most lines with formation temperature above  $\approx 10^6$  K are still clearly detectable above the background (filled circles in Figure 5). For this discussion, we are only interested

in a few, relatively strong lines (see following sections); those lines are still measurable up to at least  $r \approx 1.2 R_{\odot}$  or beyond (as is the case for the Mg x 62.5 nm, Mg ix 36.8 nm, or Si xii 52.1 nm lines). The same analysis can be applied to polar coronal holes, leading to similar results, although with larger uncertainties due to lower count rates in coronal lines.

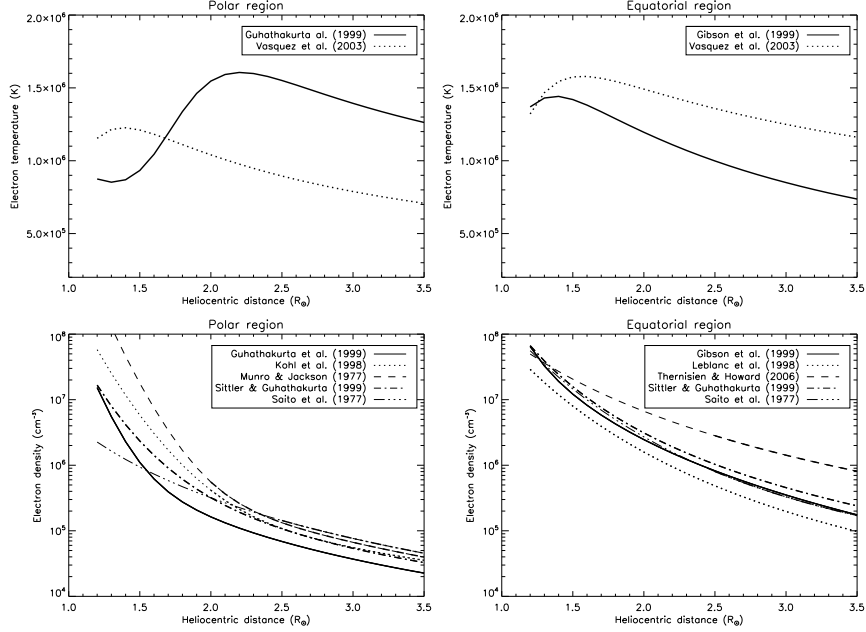


**Figure 6.** Electron temperature (top panels) and density (bottom panels) models in polar coronal holes (left panels) and in equatorial streamers (right panels); the lines representing the different models are thicker in the corresponding domain of validity.

As mentioned in Section 1, these measured radiances will be used to constrain various semiempirical models of the corona found in literature. A summary of the plasma parameters from those models is shown in Figure 6; the models are described in more detail in Section 3.

### 2.3. Temperatures and Densities from CDS Radiances

From the average radiance radial profiles, it is possible to obtain estimates of average temperatures and densities above the limb using line-ratio diagnostics. We selected the density-sensitive ratio Si ix 34.2/35.0 nm and the temperature-sensitive ratio Mg x 62.5 nm/Mg ix 36.8 nm, in analogy with the similar analyses of Gibson *et al.* (1999) and Fludra *et al.* (1999), based on SOHO/CDS measurements during the solar minimum in 1996. The latter temperature-sensitive ratio has the advantage that the lines are bright and from the same element.

The densities and temperatures from the observed line ratios were obtained using the CHIANTI database (Dere *et al.*, 1997), version 6 (Dere *et al.*, 2009), in particular including the new ion abundances in ionization equilibrium.



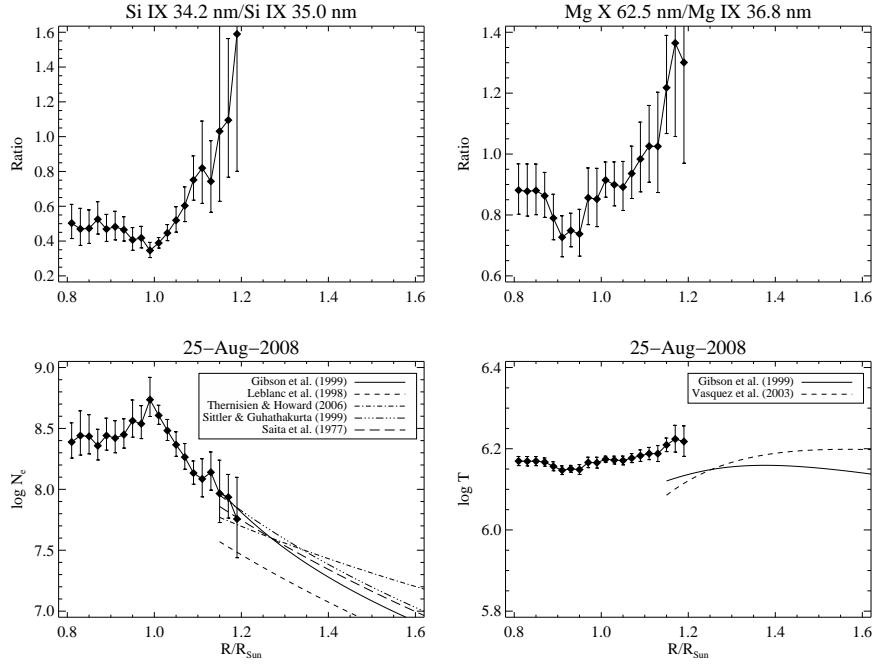


**Figure 7.** Top panels: Mean line ratios from CDS observations, for the southeast region shown in Figure 4. Bottom panels: Corresponding diagnosed quantities (left panels:  $N_e$ , right panels:  $T_e$ ), compared with various semiempirical models of streamer regions.

The line ratios measured at the base of the southeast streamer are shown in Figure 7 (top panels), while the corresponding plasma parameters, compared with density and temperature profiles from various authors, are shown in the lower panels. Figure 8 reports the same results for the polar coronal holes.

The work of Gibson *et al.* (1999) and Fludra *et al.* (1999) actually base their temperature measurement on the ratio of the lines Si XII 52.1 nm and Mg X 62.5 nm. However, those two lines may be affected by an anomalous behavior of the Li-like ions in many emission measure analyses, as described in Del Zanna, Landini, and Mason (2002). Indeed, the ratio measured in our data is at variance both with the other ratio and with the literature profiles. In polar coronal holes, in particular, that ratio yields too high a temperature, even slightly higher than in the rest of the corona. We used a photospheric mixture of abundances, as discussed in Section 3.1.3, but since both Mg and Si are elements with low first ionization potential (FIP), adopting “coronal” abundances would not significantly reduce such a discrepancy. This incongruity may be due to the anomalous behavior of Li-like ions mentioned above and discussed in Section 4.1, but also to the fact that the Si XII 52.1 nm line is weaker than the Mg X 62.5 nm line, much more so in coronal holes, and thus may possibly be affected by the stray light described in Section 2.2. With these caveats in mind, while regarding the temperature from the ratio of the two as unreliable, we will nevertheless consider for both lines the radiance radial profiles and compare them with the corresponding calculations of Section 4.

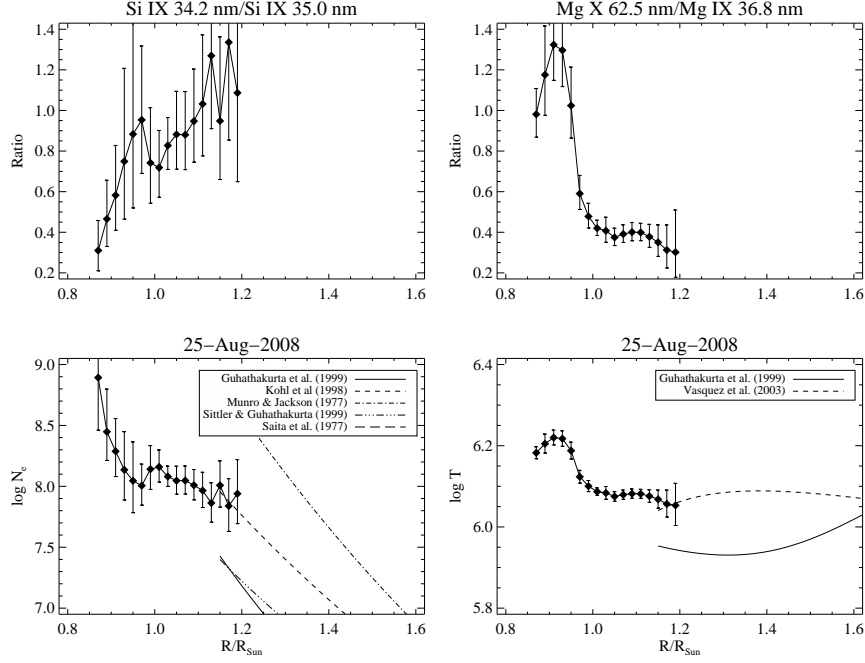


**Figure 8.** Top panels: Mean line ratios from CDS observations, for the the polar regions shown in Figure 4. Bottom panels: Corresponding diagnosed quantities (left panels:  $N_e$ , right panels:  $T_e$ ), compared with various semiempirical models of polar (coronal hole) regions.

### 2.3.1. Streamer

The density profile for the off-limb quiescent corona from the ratio Si ix 34.2/35.0 nm, if extrapolated to heliocentric distances  $r > 1.2 R_\odot$ , is in excellent agreement with the values listed by Gibson *et al.* (1999), as well as with the density profiles of Thernisien and Howard (2006), Sittler and Guhathakurta (1999), and Saito, Poland, and Munro (1977), while the profile of Leblanc, Dulk, and Bougeret (1998) gives densities too low by a factor  $\approx 3$ .

The agreement with the temperature profile given by the ratio Mg x 62.5 nm/Mg ix 36.8 nm, while still good, is somewhat less stringent, with a coronal temperature of about  $1.5 - 1.6 \cdot 10^6$  K, slightly higher than the peak value of  $1.45 \times 10^6$  K given by both Gibson *et al.* (1999) and Vásquez, van Ballegoijen, and Raymond (2003).

### 2.3.2. Polar Regions (Coronal Holes)

In polar regions, the inferred densities match much better the estimates by Kohl *et al.* (1998) than those by the other sources: Guhathakurta *et al.* (1999); Munro and Jackson (1977); Sittler and Guhathakurta (1999, 2002), and Saito, Poland, and Munro (1977). This last article gives a density  $N_e \approx 2 \times 10^6 \text{ cm}^{-3}$  at  $r/R_\odot = 1.2$ , below the lower limit of Figure 8.

The agreement of the temperature from the Mg x 62.5 nm/Mg ix 36.8 nm ratio with the profile given by Vásquez, van Ballegoijen, and Raymond (2003) is in this case excellent, and much better than with the profile of Guhathakurta *et al.* (1999).

### 3. Calculated Radiances

The calculated radiances can be divided into a collisional component and a component radiatively excited by the line radiation from the solar disk (for the He II line or other transition-region lines) or from the inner corona (for the Si XII line and other coronal lines). As an additional consistency check in the calculations, we applied the procedure described below to two other lines observed by CDS: Si XII 52.1 nm and Mg x 62.5 nm.

The collisional component of a line emissivity for the strong lines we are considering can be computed using the standard approximation of collisional excitation from the ground level followed by radiative decay.

The radiative component of the emissivity due to resonant scattering, *i.e.* the line emission due to the absorption and re-emission of photons from the lower solar atmosphere (chromosphere or near-limb corona) by ions/atoms in the corona (also known as “Doppler dimming”), has been calculated adopting the formalism of Withbroe *et al.* (1982) and Noci, Kohl, and Withbroe (1987). The relevant atomic data adopted were taken from the CHIANTI database version 6 (Dere *et al.*, 1997, 2009).

Finally, the integration of line emissivities is performed along the line of sight (LOS) over a coronal sector  $\approx 120^\circ$  wide, where a spherical symmetry is assumed. At low heights the most significant contribution to the synthesized line radiance is given by the emission near the plane of the sky (POS), because of the rapid decrease of the electron density with increasing heliocentric distance. For larger heliocentric heights, the integration path along the LOS must be larger since the electron density decreases more slowly; therefore, even the emission far from the POS contributes significantly to the line intensity. For all the heliocentric heights where the coronal-line radiances are assessed, a further increase of the integration interval involves a radiance variation  $< 5\%$ .

#### 3.1. Coronal Physical Quantities

The other ingredients needed to compute line emissivities are as follows: electron density and temperature (summarized in Figure 6), ion abundance, outflow speed of the expanding solar corona, three-dimensional (3D) velocity distribution of the coronal absorbing ions as a function of heliocentric distance and latitude, total radiance and profile of the exciting lines emitted by the disk or the lower corona. These parameters will be discussed in more detail in the following sections.

All of the physical and dynamic parameters describing the line-profile formation along the LOS are chosen by employing coronal models consistent with the observations near solar minimum, and already briefly discussed in the previous

section in the context of empirical diagnostics. In some cases, these models are extrapolated down to  $1.2 R_{\odot}$  to reach the SOHO/CDS domain of validity and at high heliocentric distances in the coronal sector  $\approx 120^{\circ}$  wide where the integration along the LOS is performed.

### 3.1.1. Electron Temperature and Density: Polar Regions

Electron densities can be determined from measurements of polarized brightness (pB) by using the inversion technique developed by van de Hulst (1950). The pB is directly related to the coronal electron density, since it depends upon the Thomson scattering of the photospheric white-light radiation by coronal electrons. The technique relies on the inversion of the equation describing the relation between the observed Thomson-scattered pB and the electron density.

Among the first attempts to infer the electron-density distribution within a polar coronal hole from pB observations with space coronagraphs, Munro and Jackson (1977) and Saito, Poland, and Munro (1977) derived electron-density radial profiles, valid from 2 to  $5 R_{\odot}$  and from 2.5 to  $5.5 R_{\odot}$ , respectively, by using data provided by the High Altitude Observatory (HAO) white-light coronagraph on *Skylab*.

More recently, Kohl *et al.* (1998) modeled the electron density in a polar coronal hole, from  $\approx 2$  to  $4 R_{\odot}$ , by measuring the linear polarization due to Thomson-scattered photospheric light with the SOHO/*Ultraviolet Coronagraph Spectrometer* (UVCS; Kohl *et al.*, 1995) white-light channel, while Sittler and Guhathakurta (1999) developed an empirical electron-density profile at the poles from *Skylab* coronagraph white-light data (Guhathakurta, Holzer, and MacQueen, 1996). The electron-density model, valid only outside  $1.16 R_{\odot}$ , was extended into interplanetary space by using electron densities derived from the *Ulysses* plasma data (Phillips *et al.*, 1995).

Quantitative information on the electron-density distribution of a coronal hole was also estimated by Guhathakurta *et al.* (1999) by combining white-light, pB observations from the SOHO/LASCO-C2 and -C3 and HAO/Mauna Loa Mark III coronagraphs with density-sensitive EUV line ratios of Si ix 35.0/34.2 nm observed by SOHO/CDS, to obtain a density profile from 1 to  $8 R_{\odot}$  for the polar coronal hole. With the assumptions that the coronal gas is locally isothermal and in radial hydrostatic equilibrium along the LOS, Guhathakurta *et al.* (1999) determined an effective (electron) temperature in polar coronal holes.

Another method for inferring the coronal electron temperature is based on *in-situ* measurements of the solar-wind charge state, which is determined in large part by the electron temperature in the inner corona, where the ionization and recombination times are still short compared to the solar-wind expansion time. The electron temperature between 1 and  $8 R_{\odot}$  derived by Ko *et al.* (1997) and Cranmer, Field, and Kohl (1999) in a polar coronal hole, from observations with *Ulysses*/SWICS, were fitted with a combination of two power laws from Vásquez, van Ballegoijen, and Raymond (2003) to give an electron-temperature model at the poles.

The above models, which differ significantly for  $r < 2 R_{\odot}$  as shown in the left panels of Figure 6, are employed in the synthesis of the radiance of the He II

30.4 nm, Si xI 30.3 nm, Si xII 52.1 nm, and Mg x 62.5 nm lines, in order to point out the sensitivity of the coronal line intensity to the density and especially to the temperature of the electrons.

### 3.1.2. Electron Temperature and Density: Equatorial Regions

Concerning the electron-density models employed in the assessment of the intensity of the He II, Si xI, Si xII, and Mg x lines at low heliographic latitudes, Saito, Poland, and Munro (1977) and Sittler and Guhathakurta (1999) (see Section 2.3) also investigated the equatorial electron-density distribution, providing models valid from 2.5 to 5.5  $R_{\odot}$  and outside 1.16  $R_{\odot}$ , respectively. The electron-density models developed by Leblanc, Dulk, and Bougeret (1998), Gibson *et al.* (1999), and Thernisien and Howard (2006) within a streamer have been considered in the analysis as well.

Leblanc, Dulk, and Bougeret (1998) derived the electron-density distribution in the ecliptic plane, from the corona to 1 AU, using observations from 13.8 MHz to a few kilohertz by the radio experiment WAVES onboard the *Wind* spacecraft. The radio technique is based on the measurement of the drift rates of type III bursts at each frequency, which allowed the authors to estimate the speed of electron streams creating the bursts, and, indirectly, an electron-density model all along the trajectory of the bursts for  $r > 1.2 R_{\odot}$ .

Gibson *et al.* (1999) modeled electron densities within a streamer structure, from 1 to 8  $R_{\odot}$ , using coronal observations of both visible white light (SOHO/LASCO-C2 and HAO/Mauna Loa Mark III coronagraphs) and extreme ultraviolet (SOHO/CDS spectrometer) emission, by way of the van de Hulst inversion.

Finally, Thernisien and Howard (2006) presented a 3D reconstruction of the electron density of a streamer, using total-brightness observations performed by SOHO/LASCO-C2 and -C3 from 2.5 to 30  $R_{\odot}$ . The radial profile of the electron density was determined via inversion techniques based on the method implemented by Hayes, Vourlidas, and Howard (2001).

The above electron-density models, which agree quite well for  $r < 1.5 R_{\odot}$  while differing significantly for larger heliocentric distances, are shown in the bottom-right panel of Figure 6. In the top-right panel of the same figure, the electron-temperature models within an equatorial streamer by Gibson *et al.* (1999) and Vásquez, van Ballegoijen, and Raymond (2003) are shown.

From the inferred density profile, Gibson *et al.* (1999) deduced a hydrostatic temperature profile inside the streamer from the ideal gas law,  $T = (1 + 2\alpha)/(2 + 3\alpha) \times P/(n_e k_B)$ . Here  $\alpha = 0.1$  is the helium number density relative to hydrogen and  $P$  is the total thermal pressure, which, in the assumption that the plasma in the streamer is in hydrostatic equilibrium, is exactly balanced by gravity.

Because of the high density and low outflow velocity in streamers, protons and electrons are expected to be in thermal equilibrium with each other, so the electron temperature at the Equator can be assumed to be equal to the proton temperature. Furthermore, because of the rapid charge exchange between protons and neutral-hydrogen atoms, the hydrogen temperature, which can be estimated by measuring the width of the Ly $\alpha$  coronal emission line profile,

reflects the proton temperature at radii up to  $3 R_{\odot}$  in the polar regions and even higher in the equatorial regions (Withbroe *et al.*, 1982). Hence, Vásquez, van Ballegooijen, and Raymond (2003) derived an electron-temperature model within a streamer, by fitting (with a combination of two power laws) SOHO/UVCS low-latitude observations of the Ly  $\alpha$  line width (Raymond *et al.*, 1997).

### 3.1.3. Elemental Abundances

Because of the numerous of results on elemental abundances derived from various types of data provided by different instruments and under different physical conditions (solar energetic particle (SEP) observations, flare observations, spectroscopy of closed coronal loops, corotating interaction region analysis), it is often quite difficult to know which data set should be used to ensure consistency with the observations.

In this work, we adopted the set of photospheric abundances listed in Asplund *et al.* (2009); more specifically,  $A_{\text{He}} = 0.085$ ,  $A_{\text{Si}} = 3.24 \times 10^{-5}$ , and  $A_{\text{Mg}} = 3.98 \times 10^{-5}$ . To a first approximation, no variation of the elemental abundances with heliographic latitude and heliocentric distance is considered here; *i.e.* the elemental abundances are assumed to be equal in the polar and equatorial regions and to be constant throughout the analyzed height range. However, some observations indicate that equatorial regions at the solar minimum include a “coronal” mix of elements, *i.e.* elements of low FIP such as Si and Mg should be more abundant by a factor of several.

This dichotomy between abundances in the equatorial and polar regions is well established from *in-situ* measurements (*e.g.*, von Steiger *et al.* 2000, who give a FIP bias of two–three), but is probably a rather coarse schematization for the corona closer to the Sun (*e.g.*, Raymond *et al.*, 1997), a region for which there are various contradictory measurements. We mention, for instance, Feldman *et al.* (1998) who considered abundances in the low corona above polar coronal holes and the quiet Sun during minimum. They measured a FIP enhancement above the quiet Sun of about four between, *e.g.*, Mg and Ne. On the other hand, Young (2005) instead found the Mg/Ne ratio to be nearly photospheric. Moreover, the He abundance is rather variable even in the solar wind; for instance, there are measurements indicating  $A_{\text{He}}$  of the order of 0.05 in the fast solar wind (*e.g.*, Bochsler, 1998).

In any case, the line radiances scale linearly with the elemental abundance, so that it is easy to evaluate the effect of a given chemical mixture on the calculations discussed in this article.

### 3.1.4. Outflow Speed of the Expanding Coronal Plasma

In order to quantify the Doppler dimming of the resonant scattering process due to the expansion of the solar corona, a semiempirical model for the outflow speed of the fast solar wind has been employed in the analysis.

The model has been derived so as to be compatible with the previous results by Antonucci *et al.* (2004) at low heliocentric distances and with the asymptotic outflow velocity  $v_{\infty} \approx 750 - 800 \text{ km s}^{-1}$ , which is definitely achieved at  $\approx 20 R_{\odot}$ .

(Breen *et al.*, 1996), but probably even at  $\approx 8 R_{\odot}$ , according to interplanetary-scintillation observations (Grall, Coles, and Klinglesmith, 1995). In particular, the model is consistent with the outflow velocity of the oxygen component of the fast solar wind derived by Telsoni, Antonucci, and Dodero (2007a,b), from the intensity ratio of the Doppler dimmed O VI 103.19, 103.76 nm doublet lines observed with SOHO/UVCS in polar coronal holes, from 1.5 out to  $5 R_{\odot}$ , during the 1996–1997 solar minimum.

Concerning the flow speed in the streamer regions, Sheeley *et al.* (1997) developed a model for the slow solar wind from 2 to  $30 R_{\odot}$ , by tracking the birth and outflow of outward moving density inhomogeneities observed with the SOHO/LASCO-C2 and -C3 coronagraphs during sunspot-minimum conditions in 1996. The authors concluded that those coronal moving features were passively tracing the slow wind, which originates above the cusps of helmet streamers at about  $3\text{--}4 R_{\odot}$  and radially outflows with a nearly constant acceleration of about  $4 \text{ m s}^{-2}$ , according to a parabolic speed profile. This profile is consistent with an isothermal solar wind expansion at a temperature of about 1.1 MK and a sonic point near  $5 R_{\odot}$ . This model is also consistent with the results found by Antonucci, Abbo, and Dodero (2005) from SOHO/UVCS data, in the analysis of the slow wind and magnetic topology in the solar minimum corona in 1996–1997.

### 3.1.5. Intensity Profiles from the Chromosphere and Lower Corona

In order to estimate the optical pumping by disk radiation of the lines considered in this article, we use the average USUN CDS line profiles; for the He II 30.4 and Si XI 30.3 nm lines the average disk line radiances are  $5.39 \times 10^3$  and  $1.04 \times 10^2 \text{ erg cm}^{-2} \text{ s}^{-1} \text{ sr}^{-1}$ , respectively, while for the Mg X 62.5 and Si XII 52.1 nm lines the measured average radiances are 50.4 and  $3.81 \text{ erg cm}^{-2} \text{ s}^{-1} \text{ sr}^{-1}$ , respectively. We remark again that the Si XI 30.3 nm disk radiance has been taken into account for the calculation of the pumping of both the Si XI and the He II lines in the corona.

In all cases, a constant intensity and shape of the exciting line profiles across the solar disk is assumed, *i.e.* no limb brightening or darkening has been considered.

### 3.1.6. 3D Velocity Distribution of the Coronal Helium Ions

In order to quantify the number of chromospheric photons scattered by the  $\text{He}^+$  ions in the extended corona, we account for the width of the coronal absorption profile of the helium ions along the direction of the incident radiation  $[\mathbf{n}]$ , which is related to the helium kinetic temperature  $[T_{\text{He},n}]$ . The velocity distribution of the absorbing helium ions sets the assumed degree of anisotropy. In particular, if  $T_{\text{He},n} = T_e$  the degree of anisotropy is maximum, while if  $T_{\text{He},n} = T_{\text{He,LOS}}$ , where  $T_{\text{He,LOS}}$  is the helium temperature along the LOS, the ion velocity distribution is isotropic. There is some uncertainty related to the temperature anisotropy assumed in the analysis. Moreover, further uncertainty is introduced since the helium temperature along the LOS has not yet been directly measured. In the synthesis of the radiance of the He II 30.4 nm line, it is assumed that the

helium temperature along the LOS reflects that of the hydrogen atoms, both in polar and equatorial regions. In particular, a semiempirical model of the helium temperature has been derived from the hydrogen temperature inferred by measuring the width of the Ly  $\alpha$  coronal emission line profile observed with the SOHO/UVCS spectrometer during the 1996–1997 minimum (Antonucci, Abbo, and Dodero, 2005). Since there is no evidence for anisotropic velocities of helium ions, we assume here that they have an isotropic velocity distribution both at high and low heliographic latitudes. Note that the above assumptions do not affect significantly the He II intensity results for heliocentric distances smaller than  $2 R_{\odot}$ , where the collision excitation dominates, whereas at larger heliocentric distances they lead to uncertainties of less than 30%.

#### 4. Discussion

The radiances computed as described in Section 3 can be compared with the radiances measured as described in Section 2, in the region  $r/R_{\odot} \approx 1.2$ , delimiting the respective domains of validity. We again remark that while some coronal temperature and density models are already given down to that value of heliocentric distance (as in, *e.g.*, Gibson *et al.*, 1999), in other cases the values shown here are extrapolated below their domain of validity (as it is the case of data from, *e.g.*, Thernisien and Howard, 2006), and therefore should be treated with caution (see also Figure 6).

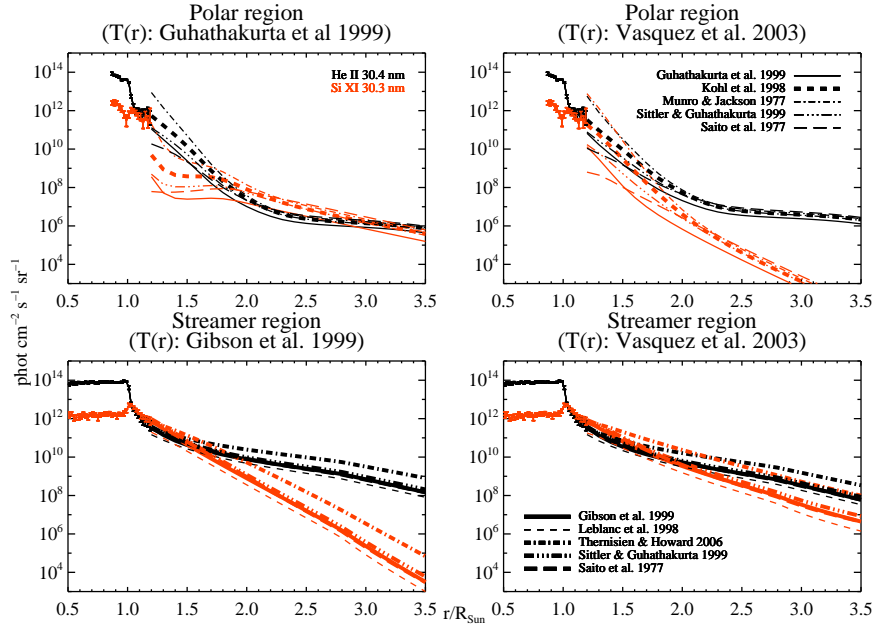


**Figure 9.** Comparison of radiances measured from SOHO/CDS and computed adopting various model profiles of temperature and density in the corona. The lines shown here are: He II 30.4 nm (black) and Si XI 30.3 nm (red).



The comparison for the lines He II 30.4 nm and Si XII 30.3 nm is shown in Figure 9; for that comparison, note that measured He II 30.4 nm radiances are dominated by stray light almost everywhere above the limb, and thus constitute only an upper limit for the theoretical calculations. Figure 10 shows instead the measured and computed radiances of the Si XII 52.1 nm and Mg X 62.5 nm lines. As noted in Section 2.3, the former line is also likely to be affected to some extent by instrumental stray light, especially in the corona above polar holes; in those cases, its measured radiances can be regarded as upper limits.

Note that we have also examined the relative weight of the collisional and radiative components in the various computed lines. Normally, it is assumed that collisional excitation dominates in the low corona for most ions/atoms, while further away from the Sun both radiative and collisional excitation may be important. In practice, we found that the Si XII 52.1 nm line is practically purely collisional, while for the Si XII 30.3 nm and Mg X 62.5 nm lines the radiative contribution is not always completely negligible, but is at most of the order of 30–40% (at  $\approx 3 r/R_\odot$ ), depending on the specific set of approximations used (see also Withbroe *et al.*, 1982). However, the He II 30.4 nm line has a negligible collisional component and can thus be considered purely radiative, and therefore dependent on the details of the flow velocity in the corona, among other things (Doppler dimming).

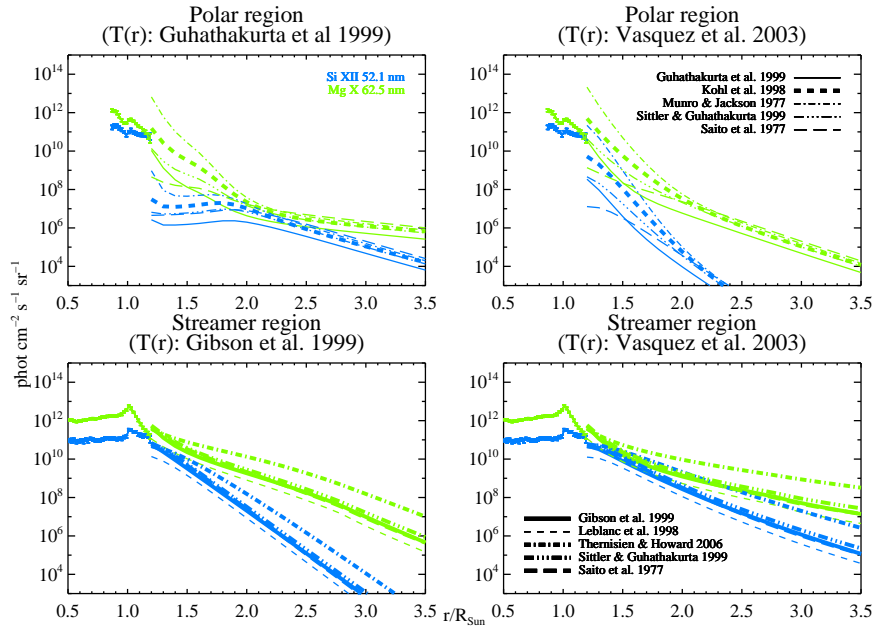


**Figure 10.** Comparison of radiances measured from SOHO/CDS and computed adopting various model profiles of temperature and density in the corona. The lines shown here are: Si XII 52.1 nm (blue) and Mg X 62.5 nm (green).

#### 4.1. Streamer

The comparison between computed and measured radiances in the streamer region of the data set considered here is shown in the lower panels of Figures 9 and 10. Taking into account that the radiances of the He II 30.4 nm line above the limb are strongly affected by stray light, all calculations appear to reasonably match the observations. In particular, both the temperature profiles of Gibson *et al.* (1999) and Vásquez, van Ballegooijen, and Raymond (2003) reproduce the radiances in the corona observed by CDS. This is not entirely surprising, since both temperature profiles set their peak coronal temperature at  $\approx 1.5 \times 10^6$  K, a value close to the one inferred from CDS line ratios (see Figure 7). Moreover, almost all of the density profiles considered here produce radiances that can be considered in accordance with CDS observations. Nevertheless, in the following, on the basis of the analysis of Section 2.3, we will exclude the calculations obtained with the density profile of Leblanc, Dulk, and Bougeret (1998) (short-dashed lines in the figures).

Overall, the agreement between computed and measured radiances is considered reasonable, but the computed Mg x 62.5 nm seems to be a factor  $\approx$  two higher than the measurements. A better agreement would be found if the density profile of Leblanc, Dulk, and Bougeret (1998) were adopted, but that density profile is incompatible with the densities inferred from the Si ix line ratio, as mentioned above.

The problem with the Mg x 62.5 nm line is not completely unexpected: discrepancies between observed and predicted radiances/irradiance (assuming ionization equilibrium and some form of emission-measure modeling) in lines from the Na- and Li-like ions have appeared since the beginning of space observations. This has been noted occasionally in the literature. The problem is actually more complex and pervasive than originally understood, as explained in Del Zanna (1999).

Del Zanna (1999) found with differential emission measure (DEM) analysis that Mg x lines in the quiet Sun were overestimated by a factor of 1.6. Del Zanna (1999) reconsidered various historical records (*e.g.*, Judge *et al.*, 1995) and found that the problem is present in all data sets. The lines from Li-like ions formed in the transition region tend to be underestimated by a large factor, while those formed at coronal temperatures are overestimated. Finally, Del Zanna, Bromage, and Mason (2001a) reanalyzed *Skylab* data and found that Mg x lines were overestimated by a factor of ten.

For a short review on the subject, see Del Zanna, Landini, and Mason (2002). We only mention here that the problem can perhaps be ascribed to the ion-balance calculations, although some of the explanations proposed (*e.g.* the density dependence of dielectronic recombination rates) probably do not apply to these coronal observations.

#### 4.2. Polar Regions (Coronal Holes)

From the upper panels of Figures 9 and 10, it is clear that Si xI 30.3 nm and Si xII 52.1 nm radiances computed with the temperature profile of Guhathakurta *et al.*

(1999) strongly underestimate (even by two or more orders of magnitude) the observed values in the lower corona, regardless of the density profile adopted. This is an independent confirmation of the same finding discussed in Section 2.3 (see also Figure 8). Also considering the upper limits given by the He II 30.4 nm line, and the radiances of the Mg x 62.5 nm line, the radiance profiles that best match the observations are instead those obtained with the Vázquez, van Ballegooijen, and Raymond (2003) temperatures and the Kohl *et al.* (1998) densities. As discussed in Section 2.3, these are also the  $T_e(r)$  and  $N_e(r)$  profiles, respectively, that best match the line ratios in Figures 7 and 8.

#### 4.3. The Ratio Si XI 30.3 nm/He II 30.4 nm

From the measured and computed values of the radiances of the Si XI 30.3 nm and He II 30.4 nm lines, we can then proceed to determine the range of values of their ratios in the quiescent solar corona. In Figure 11 we show the observed ratio from the CDS observations, up to  $1.2 R_\odot$ . Recalling once again that the He II 30.4 nm line is affected by stray light above the limb, the corresponding values of the ratio shown in that figure are actually only upper limits.

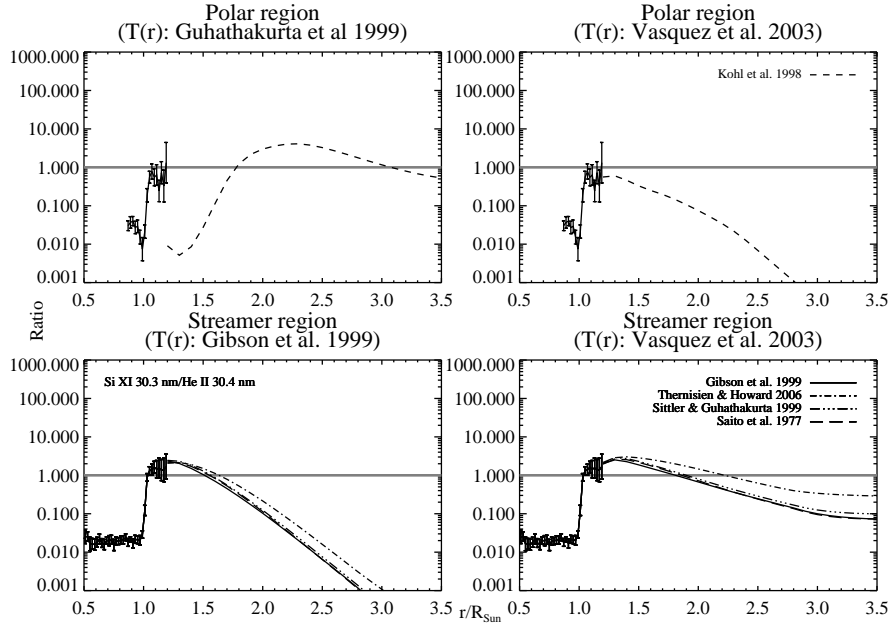


**Figure 11.** Ratio Si XI 30.3 nm/He II 30.4 nm, both observed by CDS ( $r/R_\odot < 1.2$ ) and computed ( $r/R_\odot > 1.2$ ). The horizontal grey line indicates, for clarity, the level at which the two lines have the same radiance.

For the polar regions, we show the ratio computed with the temperatures of Vázquez, van Ballegooijen, and Raymond (2003) and the densities of Kohl *et al.* (1998) (upper right panel of Figure 11), because those profiles produce a better match with observations, as discussed in the previous section. The result is that the helium Ly  $\alpha$  dominates the nearby Si XI resonance line even in the lower

corona, down to  $\approx 1.2 R_{\odot}$ . However, we also show the results obtained with the temperature profile of Guhathakurta *et al.* (1999) (upper left panel of Figure 11), even though it clearly underestimates the radiances of several coronal lines in the lower corona, to show the effect of the temperature profile on these results.

In the case of a streamer above  $\approx 1.5 R_{\odot}$ , the temperature profile also has a strong effect, especially on the Si x1 30.3 nm line (see Figure 9). On the other hand, the details of the density profile are much less important in determining the value of the ratio Si x1 30.3 nm/He II 30.4 nm. However, in all cases the Si x1 30.3 nm line dominates over the He II 30.4 nm line in the corona below  $\approx 1.5 R_{\odot}$ , and even above (at least up to  $\approx 2.3 R_{\odot}$ ) if we adopt the temperature profile of Vásquez, van Ballegooijen, and Raymond (2003).

As mentioned in Section 3.1, the above results are based on the assumption of a photospheric mixture of elements.

In polar holes, the Si abundance should not be different, but He might be depleted by a factor  $\approx$  two with respect to the photosphere. If so, the ratio Si x1 30.3 nm/He II 30.4 nm could increase above unity for heliocentric distances below  $\approx 1.5 R_{\odot}$  (considering only the temperature profile of Vásquez, van Ballegooijen, and Raymond 2003).

However, in quiescent equatorial streamers it is possible that the abundance of a low-FIP element like Si is enhanced with respect to a high-FIP element like He, by a factor of the order of three–four. Such an enhancement would extend considerably the region where the Si x1 30.3 nm dominates the He II 30.4 nm line. But the agreement with the radiances shown in Figure 9 would also be less satisfactory: increasing the abundance in streamers of the low-FIP elements Si and Mg would perhaps improve the agreement for the Si x11 52.1 line, at the expense of a worse match with observations for the Si x1 30.3 and Mg x 62.5 lines. Clearly, in this case invoking for example a “filling factor” would not mitigate the problem.

## 5. Conclusions

Our results indicate that the Si x1 30.3 nm line is important compared to the He II 30.4 nm in the corona below  $\approx 2.0 R_{\odot}$ , to the point of being the dominant source of emission in the 30.4 nm band in streamers, less likely so in polar regions (coronal holes). Beyond that distance, different temperature profiles predict a generally rapid decline of that contribution, mainly because of the strong dependence of the Si x1 resonance line on temperature. For instance, the model by Vásquez, van Ballegooijen, and Raymond (2003) predicts a non-negligible contribution of the Si x1 30.3 nm up to  $\approx 3.0, 3.5 R_{\odot}$ , whereas the temperature profile from Gibson *et al.* (1999) implies a much more rapid drop of that line with heliocentric distance.

However, the density profile has a relatively less important role in determining the emission ratio Si x1/He II in the extended corona.

There is one important caveat about the Si x1 30.3 nm calculations. The CHIANTI atomic data include rates for collisional excitation by electrons that were not calculated, but interpolated along the Be-like sequence, and the same

occurred for Mg ix. Del Zanna, Rozum, and Badnell (2008) performed the first scattering calculation for Mg ix, and found significant differences in the emissivities of key lines when compared to the results from the interpolated data. The resonance line was only affected by about 10%, so large corrections to the Si xi 30.3 nm are not expected. However, we will know this for sure only when new calculations (in progress by GDZ) become available.

As a consistency check for our calculations, we also computed the radiances for a few representative lines observed by CDS, taking into account both the collisional excitation and the radiative pumping by the disk radiation, using average radiances from the same CDS data. Here we only show the results for the Mg x 62.5 nm and Si xii 52.1 nm lines. The overall agreement between calculations and observations is reasonable; there are some discrepancies in the case of the Mg x line, but they can be attributed to a known problem (but of uncertain origin) in the emissivity calculations for that line.

We recall that the observed radiances shown here were derived adopting the latest radiometric calibration for the CDS/NIS, including the correction for the long-term decay in sensitivity of the instrument (Del Zanna *et al.*, 2010, and references therein). Since most, if not all, previous analyses done merging near-limb EUV data and extended corona measurements rely on line ratios only (*e.g.*, Gibson *et al.*, 1999), we note the generally good to excellent match between observed and computed *absolute* radiances in the strongest coronal lines.

Finally, our results were obtained adopting photospheric abundances from Asplund *et al.* (2009). Adopting coronal abundances would alter somewhat the results, especially for  $r < 2.0 R_{\odot}$ . However, in that region abundance measurements are less well established than, for instance, *in-situ* wind measurements: the effect of abundance variations should thus be considered as an additional source of uncertainty in the ratio Si xi 30.3 nm/He ii 30.4 nm.

In summary, it is true that the diagnostic potential of narrowband imaging around 30.4 nm in the extended corona is high. In particular, radiative excitation of the main line in the band, He ii 30.4 nm, from disk emission of either the same line or of the nearby Si xi 30.3 nm line, can provide a useful tool for diagnosing radial velocities. However, the full diagnostic potential of this band can only be fulfilled if it is possible to place constraints on the possible “contamination” from coronal Si xi 30.3 nm emission. In particular, we have shown that the ratio Si xi 30.3 nm/He ii 30.4 nm is very sensitive to the specific temperature profile adopted for the corona, which is normally rather uncertain.

A corollary of these calculations is that the diagnostic potential of narrowband observations in the 30.4 nm band in critical regions of the corona ( $< 3 R_{\odot}$ ) can only be fully exploited if aided by spectroscopic observations capable of disentangling the Si xi contribution from the He ii emission. Alternatively, if one could find a way to independently determine the coronal temperature profile (the density profile is much less critical in this respect), perhaps it could be aided through simultaneous visible light imaging. Both approaches will be feasible with METIS onboard *Solar Orbiter*.

**Acknowledgements** This work is part of the scientific activities supporting the development of METIS, and as such has been supported in part (Italy) by ASI-INAF contract

I/43/10/0; further support came from ASI-INAF contracts I/05/07/0 and I/023/09/0. GDZ acknowledges support from SFTC (UK) via the Advanced Fellowship Programme. SOHO is a project of international cooperation between ESA and NASA. CDS was built and operated by a consortium led by the Rutherford Appleton Laboratory (RAL), which includes UCL/Mullard Space Science Laboratory, NASA/ Goddard Space Flight Center, Max Planck Institute for Extraterrestrial Physics, Garching, and Oslo University. Finally, we wish to thank the referee for useful comments and suggestions on the manuscript.

## References

- Andretta, V., Del Zanna, G., Jordan, S.D.: 2003, *Astron. Astrophys.* **400**, 737. doi:10.1051/0004-6361:20021893.
- Antonucci, E., Abbo, L., Doderò, M.A.: 2005, *Astron. Astrophys.* **435**, 699. doi:10.1051/0004-6361:20047126.
- Antonucci, E., Doderò, M.A., Giordano, S., Krishnakumar, V., Noci, G.: 2004, *Astron. Astrophys.* **416**, 749. doi:10.1051/0004-6361:20031650.
- Asplund, M., Grevesse, N., Sauval, A.J., Scott, P.: 2009, *Ann. Rev. Astron. Astrophys.* **47**, 481. doi:10.1146/annurev.astro.46.060407.145222.
- Bochsler, P.: 1998, *Space Sci. Rev.* **85**, 291. doi:10.1023/A:1005114920154.
- Breen, A.R., Coles, W.A., Grall, R.R., Klinglesmith, M.T., Markkanen, J., Moran, P.J., Tegid, B., Williams, P.J.S.: 1996, *Ann. Geophys.* **14**, 1235. doi:10.1007/s00585-996-1235-8.
- Brueckner, G.E., Howard, R.A., Koomen, M.J., Korendyke, C.M., Michels, D.J., Moses, J.D., Socker, D.G., Dere, K.P., Lamy, P.L., Llebaria, A., Bout, M.V., Schwenn, R., Simnett, G.M., Bedford, D.K., Eyles, C.J.: 1995, *Solar Phys.* **162**, 357. doi:10.1007/BF00733434.
- Cranmer, S.R., Field, G.B., Kohl, J.L.: 1999, *Astrophys. J.* **518**, 937. doi:10.1086/307330.
- Del Zanna, G.: 1999, *PhD thesis*, Univ. Central Lancashire.
- Del Zanna, G., Andretta, V.: 2011, *Astron. Astrophys.* **528**, A139. doi:10.1051/0004-6361/201016106.
- Del Zanna, G., Bromage, B.J.I., Mason, H.E.: 2001a, In: Wimmer-Schweingruber, R.F. (ed.) *Solar and Galactic Composition: A Joint SOHO/ACE workshop*, **CS-598**, AIP, Woodbury, New York, 59. doi:10.1063/1.1433979.
- Del Zanna, G., Landini, M., Mason, H.E.: 2002, *Astron. Astrophys.* **385**, 968. doi:10.1051/0004-6361:20020164.

- Del Zanna, G., Rozum, I., Badnell, N.R.: 2008, *Astron. Astrophys.* **487**, 1203. doi:10.1051/0004-6361:200809998.
- Del Zanna, G., Bromage, B.J.I., Landi, E., Landini, M.: 2001b, *Astron. Astrophys.* **379**, 708. doi:10.1051/0004-6361:20011220.
- Del Zanna, G., Andretta, V., Chamberlin, P.C., Woods, T.N., Thompson, W.T.: 2010, *Astron. Astrophys.* **518**, A49. doi:10.1051/0004-6361/200912904.
- Delaboudinière, J.-P., Artzner, G.E., Brunaud, J., Gabriel, A.H., Hochedez, J.F., Millier, F., Song, X.Y., Au, B., Dere, K.P., Howard, R.A., Kreplin, R., Michels, D.J., Moses, J.D., Defise, J.M., Jamar, C., Rochus, P., Chauvineau, J.P., Marioge, J.P., Catura, R.C., Lemen, J.R., Shing, L., Stern, R.A., Gurman, J.B., Neupert, W.M., Maucherat, A., Clette, F., Cugnon, P., van Dessel, E.L.: 1995, *Solar Phys.* **162**, 291. doi:10.1007/BF00733432.
- Dere, K.P., Landi, E., Mason, H.E., Monsignori Fossi, B.C., Young, P.R.: 1997, *Astron. Astrophys. Suppl.* **125**, 149. doi:10.1051/aas:1997368.
- Dere, K.P., Landi, E., Young, P.R., Del Zanna, G., Landini, M., Mason, H.E.: 2009, *Astron. Astrophys.* **498**, 915. doi:10.1051/0004-6361/200911712.
- Feldman, U., Schühle, U., Widing, K.G., Laming, J.M.: 1998, *Astrophys. J.* **505**, 999. doi:10.1086/306195.
- Fineschi, S.: 2006, In: *36th COSPAR Scientific Assembly, COSPAR, Plenary Meeting* **36**, 3347.
- Fineschi, S., Korendyke, C.M., Moses, J.D., Thomas, R.J.: 2004, In: Mather, J.C. (ed.) *Optical, Infrared, and Millimeter Space Telescopes*, **CS-5487**, SPIE, 1165. doi:10.1117/12.549417.
- Fludra, A., Del Zanna, G., Alexander, D., Bromage, B.J.I.: 1999, *J. Geophys. Res.* **104**, 9709. doi:10.1029/1998JA900033.
- Gibson, S.E., Fludra, A., Bagenal, F., Biesecker, D., Del Zanna, G., Bromage, B.: 1999, *J. Geophys. Res.* **104**, 9691. doi:10.1029/98JA02681.
- Grall, R.R., Coles, W.A., Klingle-Smith, M.T.: 1995, In: Winterhalter, D., Neugebauer, M., Kurth, W.S., Habbal, S.R., Gosling, J.T. (eds.) *Solar Wind Eight*, **CS-382**, AIP, Woodbury, New York, 61.
- Guhathakurta, M., Holzer, T.E., MacQueen, R.M.: 1996, *Astrophys. J.* **458**, 817. doi:10.1086/176860.
- Guhathakurta, M., Fludra, A., Gibson, S.E., Biesecker, D., Fisher, R.: 1999, *J. Geophys. Res.* **104**, 9801. doi:10.1029/1998JA900082.

- Harrison, R.A., Sawyer, E.C., Carter, M.K., Cruise, A.M., Cutler, R.M., Fludra, A., Hayes, R.W., Kent, B.J., Lang, J., Parker, D.J., Payne, J., Pike, C.D., Peskett, S.C., Richards, A.G., Gulhane, J.L., Norman, K., Breeveld, A.A., Breeveld, E.R., Al Janabi, K.F., McCalden, A.J., Parkinson, J.H., Self, D.G., Thomas, P.D., Poland, A.I., Thomas, R.J., Thompson, W.T., Kjeldseth-Moe, O., Brekke, P., Karud, J., Maltby, P., Aschenbach, B., Bräuninger, H., Kühne, M., Hollandt, J., Siegmund, O.H.W., Huber, M.C.E., Gabriel, A.H., Mason, H.E., Bromage, B.J.I.: 1995, *Solar Phys.* **162**, 233. doi:10.1007/BF00733431.
- Hayes, A.P., Vourlidas, A., Howard, R.A.: 2001, *Astrophys. J.* **548**, 1081. doi:10.1086/319029.
- Jordan, S.D., Brosius, J.W.: 2007, In: Heinzel, P., Dorotovič, I., Rutten, R.J. (eds.) *The Physics of Chromospheric Plasmas*, **CS-368**, Astron. Soc. Pacific, San Francisco, 183.
- Judge, P.G., Woods, T.N., Brekke, P., Rottman, G.J.: 1995, *Astrophys. J. Lett.* **455**, L85. doi:10.1086/309815.
- Ko, Y.-K., Fisk, L.A., Geiss, J., Gloeckler, G., Guhathakurta, M.: 1997, *Solar Phys.* **171**, 345.
- Kohl, J.L., Esser, R., Gardner, L.D., Habbal, S., Daigneau, P.S., Dennis, E.F., Nystrom, G.U., Panasyuk, A., Raymond, J.C., Smith, P.L., Strachan, L., van Ballegooijen, A.A., Noci, G., Fineschi, S., Romoli, M., Ciaravella, A., Modigliani, A., Huber, M.C.E., Antonucci, E., Benna, C., Giordano, S., Tondello, G., Nicolosi, P., Naletto, G., Pernechele, C., Spadaro, D., Poletto, G., Livi, S., von der Lühe, O., Geiss, J., Timothy, J.G., Gloeckler, G., Allegra, A., Basile, G., Brusa, R., Wood, B., Siegmund, O.H.W., Fowler, W., Fisher, R., Jhabvala, M.: 1995, *Solar Phys.* **162**, 313. doi:10.1007/BF00733433.
- Kohl, J.L., Noci, G., Antonucci, E., Tondello, G., Huber, M.C.E., Cranmer, S.R., Strachan, L., Panasyuk, A.V., Gardner, L.D., Romoli, M., Fineschi, S., Dobrzycka, D., Raymond, J.C., Nicolosi, P., Siegmund, O.H.W., Spadaro, D., Benna, C., Ciaravella, A., Giordano, S., Habbal, S.R., Karovska, M., Li, X., Martin, R., Michels, J.G., Modigliani, A., Naletto, G., O’Neal, R.H., Pernechele, C., Poletto, G., Smith, P.L., Suleiman, R.M.: 1998, *Astrophys. J. Lett.* **501**, L127. doi:10.1086/311434.
- Leblanc, Y., Dulk, G.A., Bougeret, J.-L.: 1998, *Solar Phys.* **183**, 165.
- Munro, R.H., Jackson, B.V.: 1977, *Astrophys. J.* **213**, 874. doi:10.1086/155220.
- Noci, G., Kohl, J.L., Withbroe, G.L.: 1987, *Astrophys. J.* **315**, 706. doi:10.1086/165172.
- Phillips, J.L., Bame, S.J., Barnes, A., Barraclough, B.L., Feldman, W.C., Goldstein, B.E., Gosling, J.T., Hoogeveen, G.W., McComas, D.J., Neugebauer, M., Suess, S.T.: 1995, *Geophys. Res. Lett.* **22**, 3301. doi:10.1029/95GL03094.



- Pietarila, A., Judge, P.G.: 2004, *Astrophys. J.* **606**, 1239. doi:10.1086/383176.
- Raymond, J.C., Kohl, J.L., Noci, G., Antonucci, E., Tondello, G., Huber, M.C.E., Gardner, L.D., Nicolosi, P., Fineschi, S., Romoli, M., Spadaro, D., Siegmund, O.H.W., Benna, C., Ciaravella, A., Cranmer, S., Giordano, S., Karovska, M., Martin, R., Michels, J., Modigliani, A., Naletto, G., Panasyuk, A., Pernechele, C., Poletto, G., Smith, P.L., Suleiman, R.M., Strachan, L.: 1997, *Solar Phys.* **175**, 645. doi:10.1023/A:1004948423169.
- Saito, K., Poland, A.I., Munro, R.H.: 1977, *Solar Phys.* **55**, 121. doi:10.1007/BF00150879.
- Sheeley, N.R. Jr., Wang, Y.-M., Hawley, S.H., Brueckner, G.E., Dere, K.P., Howard, R.A., Koomen, M.J., Korendyke, C.M., Michels, D.J., Paswaters, S.E., Socker, D.G., St. Cyr, O.C., Wang, D., Lamy, P.L., Llebaria, A., Schwenn, R., Simnett, G.M., Plunkett, S., Biesecker, D.A.: 1997, *Astrophys. J.* **484**, 472. doi:10.1086/304338.
- Sittler, E.C. Jr., Guhathakurta, M.: 1999, *Astrophys. J.* **523**, 812. doi:10.1086/307742.
- Sittler, E.C. Jr., Guhathakurta, M.: 2002, *Astrophys. J.* **564**, 1062. doi:10.1086/324303.
- Telloni, D., Antonucci, E., Dodero, M.A.: 2007a, *Astron. Astrophys.* **472**, 299. doi:10.1051/0004-6361:20077083.
- Telloni, D., Antonucci, E., Dodero, M.A.: 2007b, *Astron. Astrophys.* **476**, 1341. doi:10.1051/0004-6361:20077660.
- Thernisien, A.F., Howard, R.A.: 2006, *Astrophys. J.* **642**, 523. doi:10.1086/500818.
- Thomas, R.J., Neupert, W.M.: 1994, *Astrophys. J. Supp.* **91**, 461. doi:10.1086/191944.
- Thompson, W.T., Brekke, P.: 2000, *Solar Phys.* **195**, 45.
- van de Hulst, H.C.: 1950, *Bull. Astr. Inst. Netherlands* **11**, 135.
- Vásquez, A.M., van Ballegooijen, A.A., Raymond, J.C.: 2003, *Astrophys. J.* **598**, 1361. doi:10.1086/379008.
- von Steiger, R., Schwadron, N.A., Fisk, L.A., Geiss, J., Gloeckler, G., Hefti, S., Wilken, B., Wimmer-Schweingruber, R.F., Zurbuchen, T.H.: 2000, *J. Geophys. Res.* **105**, 27217. doi:10.1029/1999JA000358.
- Wang, T., Thomas, R.J., Brosius, J.W., Young, P.R., Rabin, D.M., Davila, J.M., Del Zanna, G.: 2011, *Astrophys. J. Supp.* **197**, 32. doi:10.1088/0067-0049/197/2/32.

- Withbroe, G.L., Kohl, J.L., Weiser, H., Munro, R.H.: 1982, *Space Sci. Rev.* **33**, 17. doi:10.1007/BF00213247.
- Young, P.R.: 2005, *Astron. Astrophys.* **439**, 361. doi:10.1051/0004-6361:20052963.